Indirect method of measuring of EM field in RF-gun cavity for XFEL accelerator

PREPRINT Elektronika 50, 8 (2009) pp.193-199

K.Poźniak, T.Stanisławski, W.Zabołotny, W.Koehler, F.Stephan, S.Simrock
ISE PW, DESY

XFEL is an abbreviation for *X-Ray Free Electron Laser*. The device is used as a source of the narrow-band X-ray radiation. At present, the XFEL prototype called FLASH (*Free electron LASer in Hamburg*) is being tested. The coherent light wave is generated in an undulator from a beam of high energy electrons. Particles are accelerated in the linear accelerator (LINAC). The RF-Gun is a source of free electrons bunches. In the *Fig. 1* the simplified diagram of the RF-Gun structure if shown. Free electrons are generated by a laser pulse concentrated on the photo-cathode. Then the particles are accelerated by the EM field in the resonance cavity [2]. In order to provide reliable beam, the timespan between the laser pulse and the maximum of the cavity field gradient has to be kept constant. Moreover the beam quality of the generated electron beam is strongly dependant on electrons' energy [3]. Therefore the system of stabilisation of the field phase and amplitude is crucial for providing the laser light with good properties.

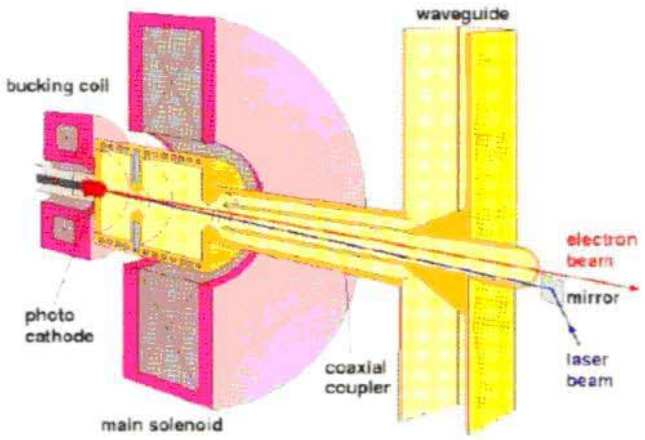

Fig. 1. Structure of RF-Gun used in PITZ and XFEL
Rys.1. Budowa działa elektronowego dla PITZ i XFEL

Structure of control system

The system of stabilisation of the cavity field is shown in the *Fig. 2*. The driving power is produced in a 10 MW klystron with two waveguides outputs. The circulators are used to separate the klystron from the rest of the waveguide system. The phase shifter is used to balance the phase shift between both waveguides. Both waves are summed in the T-Combiner. From its output the power is delivered to the cavity.

A directional coupler is installed in each waveguide. It allows to measure the complex envelope of both forward and reflected waves. All signals are downconverted and digitised.

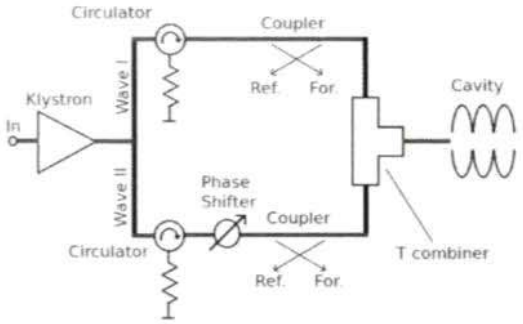

Fig. 2. The RF-Gun feeding system
Rys. 2. System zasilania mocą RF działa elektronowego

The digital samples are then transferred to the controller and used for calculation of the output IQ signals. These signals are upconverted by the vector modulator and finally used to drive the klystron, hence closing the control loop.

Stages of the control procedure

The cavity control cycle can be divided into four stages.

- Filling - the cavity is quickly filled with the EM field until it reaches the operating value.

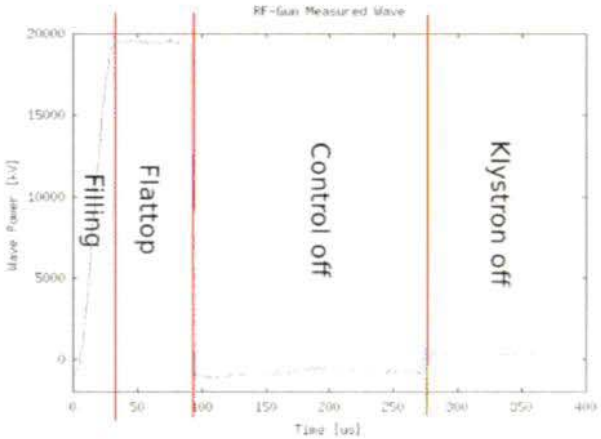

Fig. 3. The input signal behaviour for different stages of the cavity control system. During the filling the amplitude quickly rises to the nominal value. During the flattop the amplitude is stabilized. Than the control is stopped. The signal is slowly waving due to bad level of zero for the controlling signals. Finally the klystron is turned off. The signal value is equal to the offset of demodulators
Rys. 3. Zachowanie sygnałów wejściowych w różnych fazach pracy systemu sterowania wnęką. Podczas napełniania wnęki amplituda szybko rośnie do wartości roboczej. Podczas normalnej pracy amplituda jest stabilizowana. Następnie sterowanie jest wyłączane. Sygnał powoli maleje ze względu na błędny poziom zera sygnałów sterujących. W końcu klistron zostaje wyłączany. Wartość sygnału odpowiada przesunięciu zera w demodulatorach

- Flattop - The field gradient (both: amplitude and phase) is stabilised
- Control off - The klystron control signal is turned off
- RF-Gate off - The klystron does not deliver the power to the cavity

The picture showing all stages can be found in the *Fig. 3.*

Measurements of the control system parameters

The calibration of the vector demodulators

The goal of this procedure is to remove the non-orthogonality of the input vector demodulators. Moreover, the calibration should eliminate the offset signals. The idea of the calibration is based on the rotation of phase of the signal in the whole system. It can be achieved in two ways. The first solution is the rotation of the klystron input signal. The second one is the rotation of the master oscillator signal. The first solution was rejected due to nonorthogonality of the vector modulators driving the klystron input. The configuration used for the second method is shown in the *Fig. 4*. Three phase shifters were used because a single one provides only 120 degrees shift. The snapshot of the measurement signals was taken every 40 degrees of the phase shift. The taken measurements are:

- The forward and reflected waves from the directional couplers in both waveguides,
- The power of klystron wave in both waveguides,
- The klystron Set Point and Phase Settings,
- The cavity temperature.

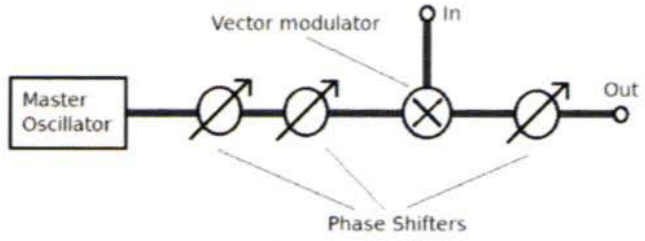

Fig. 4. Setup for the calibration of the input signals
Rys. 4. Konfiguracja systemu do kalibracji sygnałów wejściowych

Elimination of the signal offset

The measured signals are distorted by the constant offset. This additive offset may be measured after setting of the power, which drives the system, to zero. The data gathered during RF-gate closed phase are used for this purpose. The offset value is equal to the mean value of this samples.

Elimination of the nonorthogonality

In the first step the offset is subtracted. Then the signals are normalized by the square root of the klystron power. This operation is used, to ensure that signal amplitude is constant, for every position of the phase shifter. In the *Fig. 5* you can find the typical example of the signal after both operations. The third step is an optimization procedure. Data points are rotated and squeezed along the X axis in order to form a circle. The rotation angle Y and the squeezing coefficient a are optimized to minimize the goal function.

$$f(\Phi,\alpha)=\sum_{k=1}^{N}(\sqrt{x_k'^2+y_k'^2}-R)^2 \qquad (1)$$

$$f(\Phi,\alpha)=\sum_{k=1}^{N}(\sqrt{x_k'^2+y_k'^2}-R)^2 \qquad (2)$$

where: R is the mean distance of the transformed data points (x'_k,y'_k) from the origin of the coordinate system. The transformation of the data points is expressed in the form:

$$\begin{bmatrix}x_k'\\y_k'\end{bmatrix}=\begin{bmatrix}\alpha & 0\\0 & 1\end{bmatrix}\cdot\begin{bmatrix}\cos\Psi & -\sin\Psi\\\sin\Psi & \cos\Psi\end{bmatrix}\cdot\begin{bmatrix}x_k\\y_k\end{bmatrix} \qquad (3)$$

The parameters a and Y can be optimized with any minimization algorithm. The final calibration matrix C can be expressed in the form:

$$C=\begin{bmatrix}cos\Psi & \sin\Psi\\-\sin\Psi & \cos\Psi\end{bmatrix}\cdot\begin{bmatrix}\alpha & 0\\0 & 1\end{bmatrix}\cdot\begin{bmatrix}\cos\Psi & -\sin\Psi\\\sin\Psi & \cos\Psi\end{bmatrix} \qquad (4)$$

The calibrated position of the data point is calculated with the formula:

$$\begin{bmatrix}\hat{x}_k\\\hat{y}_k\end{bmatrix}=C\cdot\begin{bmatrix}x_k-x_0\\y_k-y_0\end{bmatrix} \qquad (5)$$

where x_0 and y_0 are the signal offsets. The calibration has to be performed individually for all input channels. Finally the signal has to be transformed into the complex form $\hat{p}_k$ using the simple formula:

$$\hat{p}_k=\hat{x}_k+j\cdot\hat{y}_k \qquad (6)$$

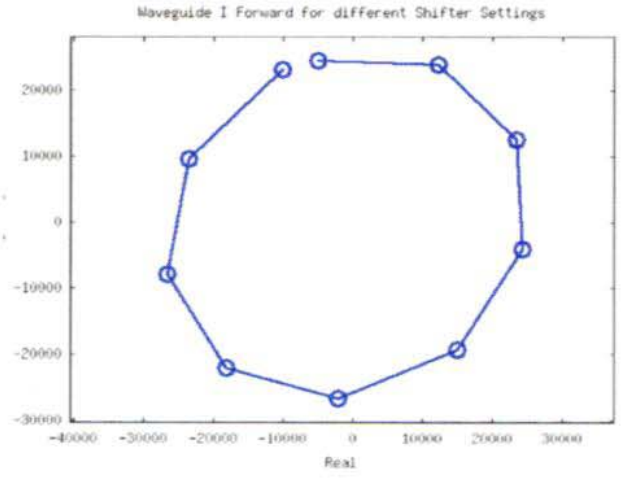

Fig. 5. The input signals after the offset elimination and the power normalization. Different points correspond to different positions of the phase shifter. The non-orthogonality of the input demodulators causes elliptical distortions. The observed signal should rotate without amplitude changes creating a circle
Rys. 5. Sygnały wejściowe po eliminacji przesunięcia zera i unormowaniu mocy. Poszczególne punkty odpowiadają różnym położeniom przesuwnika fazy. Nieortogonalność demodulatorów wejściowych wywołuje eliptyczne zniekształcenia. Wartości obserwowane sygnały powinny przemieszczać się po okręgu bez zmiany amplitudy

The temperature scanning

The method of calculation of the cavity input voltage is described. The temperature scanning is done in order to estimate the Black Box system matrices which describe the system behaviour. It is assumed that for a fixed temperature the system behaviour is defined by the formula:

$$S(T = const)\cdot\begin{bmatrix} p_{f1} \\ p_{f2} \end{bmatrix} = \begin{bmatrix} p_{r1} \\ p_{r2} \end{bmatrix} \tag{7}$$

The goal of this procedure is to analyze the system behaviour while cavity reflection coefficient *G* is changing. The G parameter is strongly dependent on the temperature. Therefore it should be stable while working with the low power of generated waves, and with the temperature stabilization. Setting of the new value of the reflection coefficient is achieved by setting of the new Set Point temperature for the temperature stabilization system.

The automatic measurement procedure

In this paragraph the procedure of automated temperature scan measurement is described. The Measurements are performed with the Matlab script. The procedure is divided into following stages:

1. Set the cavity temperature set point.
2. Wait until the temperature is stabilized.
3. Make the phase shifter scan:
   (a) Set the shifter position,
   (b) Measure the p_{f1}, p_{f2}, p_{g1} and p_{g2} by taking average value of the samples on the flattop. The samples should be previously calibrated with formula 5,
   (c) Choose different shifter position and go to the point 3a.
4. Choose different cavity temperature and go to the point 1.

The typical measurement results are found in the *Fig. 6*. It is easily noticeable that the signal vectors are rotated with the position of the shifter. The temperature is constant during this measurement.

The signals were **NOT** calibrated, and therefore the signals form ellipses while rotating phase shifter.

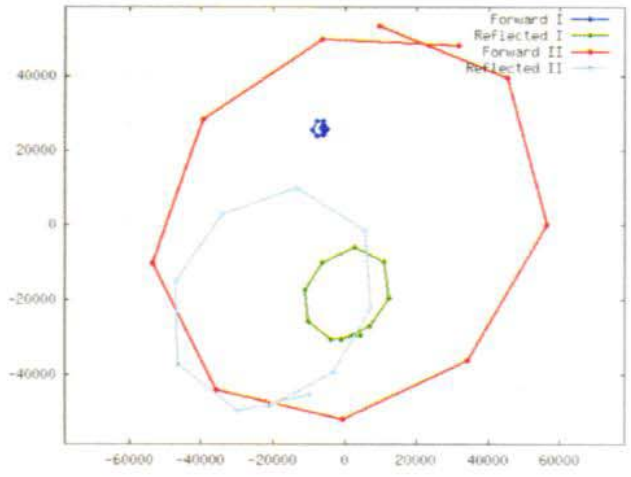

Fig. 6. The complex input signals gathered for the shifter scan during the temperature scanning. The temperature was equal to 69K
Rys. 6. Zespolone sygnały wejściowe zarejestrowane przy zmianie pozycji przesuwnika fazy podczas skanu temperaturowego. Temperatura była równa 69K

The calculation of system *S* matrix

In this section the method of calculation of the *S* matrix from the formula 7 is described. The equation can be rewritten in the form:8

$$\begin{bmatrix} s_0 & s_1 \\ s_2 & s_3 \end{bmatrix}\cdot\begin{bmatrix} p_{f1} \\ p_{f2} \end{bmatrix} = \begin{bmatrix} p_{r1} \\ p_{r2} \end{bmatrix} \tag{8}$$

However, the equation 8, for a set of measurements, taken for different positions of the shifter, can be written as a system of linear equations:910

$$\underbrace{\begin{bmatrix} p_{f1.1} & p_{f2.1} \\ \vdots & \vdots \\ p_{f1.N} & p_{f2.N} \end{bmatrix}}_{A}\cdot\begin{bmatrix} s_0 \\ s_1 \end{bmatrix} = \underbrace{\begin{bmatrix} p_{r1.1} \\ \vdots \\ p_{r1.N} \end{bmatrix}}_{b_1} \tag{9}$$

$$\underbrace{\begin{bmatrix} p_{f1.1} & p_{f2.1} \\ \vdots & \vdots \\ p_{f1.N} & p_{f2.N} \end{bmatrix}}_{A}\cdot\begin{bmatrix} s_2 \\ s_3 \end{bmatrix} = \underbrace{\begin{bmatrix} p_{r2.1} \\ \vdots \\ p_{r2.N} \end{bmatrix}}_{b_2} \tag{10}$$

Equations 9 and 10 form the overdetermined systems. Therefore there can be solved only in least squares sense. Solutions are:1112

$$\begin{bmatrix} s_0 \\ s_1 \end{bmatrix} = \left(A^T A\right)^{-1}\cdot A^T\cdot b_1 \tag{11}$$

$$\begin{bmatrix} s_2 \\ s_3 \end{bmatrix} = \left(A^T A\right)^{-1}\cdot A^T\cdot b_2 \tag{12}$$

Measurements summary

The results of experiments taken on the 14th 2009 January are found in the *Fig. 7*. The calibration matrices for all measured channels were calculated. These are used for

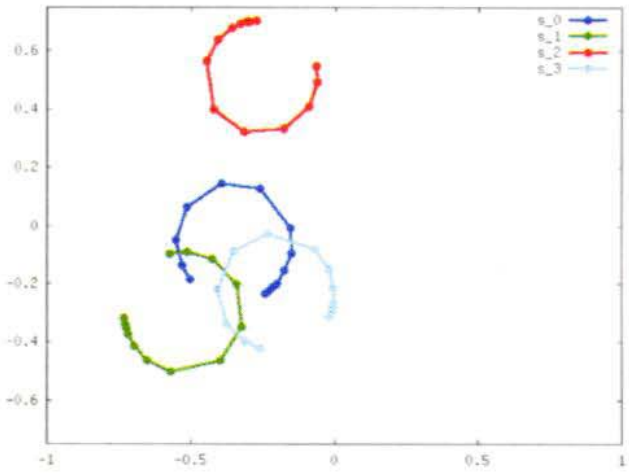

Fig. 7. The matrix coefficients for the 2-gate device. The parameters change with the temperature forming the circular shape
Rys. 7. Współczynniki macierzy dwuwrotnika. Parametry zmieniają się przy zmianie temperatury, przemieszczając się po okręgach

removal of the distortions caused by the non-orthogonality of the vector demodulators. Moreover the coefficients of the system matrix for the broad range of temperatures were measured. The *Fig. 7* shows changes of the *S* matrix coefficients. The circular shape results from the changes of the cavity reflection coefficient. Each circle corresponds to the changes of one of the *S* matrix coefficients. The *S* matrix describes the system behaviour because it reflects the mathematical relationship between all measured signals.

The mathematical model for the calculations of the EM field

The field gradient in the cavity is proportional to the voltage on the cavity entry plane. This voltage in turn is proportional to the sum of the forward and reflected waves. Therefore the knowledge of both waves allows to control the field gradient. However both signals are not observed directly in the current RF-Gun configuration. This section describes an algorithm that allows to control the cavity usign only indirect measurement of the input and output waves.

The Black Box Model

In the proposed model it is assumed that the forward and reflected signals in both waveguides are the only independent signals in the system. The Black Box model has different topology than the real one. The system diagram is shown in the *Fig. 8*. The system is driven not by the klystron but by the forward waves in both waveguides. The Black Box model is fully described by the 3 x 3 *S* parameters matrix and the reflection coefficient of the cavity Γ. Equations 13 and 14 contains all dependencies between the system signals.

$$S \cdot \begin{bmatrix} p_{f1} \\ p_{f2} \\ p_{f3} \end{bmatrix} = \begin{bmatrix} p_{r1} \\ p_{r2} \\ p_{r3} \end{bmatrix} \tag{13}$$

$$p_{f3} = \Gamma \cdot p_{r3} \tag{14}$$

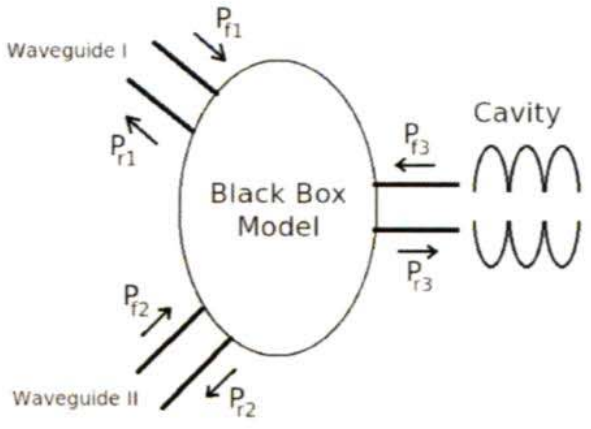

Fig. 8. The Black Box model of the RF-Gun control system.
Rys. 8. Model systemu sterowania działem elektronowym jako "czarnej skrzynki"

In the introduction it was mentioned that the sum of forward and reflected waves is proportional to the field gradient in the cavity. This section describes the method of estimation of this gradient. The signals p_{f1}, p_{f2}, p_{g1} and p_{g2} are the only measured data. The equations 13 and 14 can be transformed into the form 15.

$$\underbrace{\left[S_A + \frac{S_B \cdot S_C \cdot \Gamma}{1 - S_D \cdot \Gamma}\right]}_{S_2} \cdot \begin{bmatrix} p_{f1} \\ p_{f2} \end{bmatrix} = \begin{bmatrix} p_{r1} \\ p_{r2} \end{bmatrix} \tag{15}$$

where S_A...S_D are the submatrices of the *S* matrix of scattering parameters. Structure of the *S* matrix is:

$$S = \begin{bmatrix} S_A & S_B \\ S_C & S_D \end{bmatrix} \tag{16}$$

where:
- S_A - is a 2 x 2 matrix,
- S_B - is a 2 x 1 matrix,
- S_C - is a 1 x 2 matrix,
- S_D - is a 1 x 1 matrix (scalar).

While the *G* is constant, the system can be treated as the two gate device described by the S_2 matrix (size 2 x 2). The procedure of measurement of such matrix was described. From the equations 13 and 14 the additional formulas are derived. The forward and reflected waves on the cavity entry plane are equal to:

$$p_{f3} = \frac{\Gamma \cdot S_C}{1 - S_D \cdot \Gamma} \cdot \begin{bmatrix} p_{f1} \\ p_{f2} \end{bmatrix} \tag{17}$$

$$p_{r3} = \frac{S_C}{1 - S_D \cdot \Gamma} \cdot \begin{bmatrix} p_{f1} \\ p_{f2} \end{bmatrix} \tag{18}$$

Therefore the sum of waves on the cavity entry plane is equal to:

$$p_{f3} + p_{r3} = \frac{1 + \Gamma}{1 - S_D \cdot \Gamma} \cdot S_C \cdot \begin{bmatrix} p_{f1} \\ p_{f2} \end{bmatrix} \tag{19}$$

The above formula may not be used directly, since both *S* and *G* are in general unknown. However there exists one very special case. When cavity is strongly detuned, for example in the low temperature, then its reflection coefficient is close to $G = -1$. In this state the scattering matrix of the two gate device should be measured. This matrix is denoted as $S_2(G = -1)$. Value of this matrix is calculated from the formula 15 and is equal to:

$$p_{f3} + p_{r3} = \frac{1 + \Gamma}{1 - S_D \cdot \Gamma} \cdot S_C \cdot \begin{bmatrix} p_{f1} \\ p_{f2} \end{bmatrix} \tag{20}$$

Since $S_2(G = -1)$ and forward waves are measurable, it is possible to calculate the reflected waves for cavity replaced with the perfect short circuit. The difference between the observed reflected wave and the wave that would be observed for significantly detuned cavity is proportional to the voltage at the cavity entry. This property can be proved in the following way:

$$U_E = S_2(\Gamma = -1) \cdot \begin{bmatrix} p_{F1} \\ p_{F2} \end{bmatrix} - \begin{bmatrix} p_{R1} \\ p_{R2} \end{bmatrix} \quad (21)$$

$$= \left[S_A - \frac{S_B \cdot S_C}{1 + S_D} \right] \cdot \begin{bmatrix} p_{F1} \\ p_{F2} \end{bmatrix} - \left[S_A + \frac{S_B \cdot S_C \cdot \Gamma}{1 - S_D \cdot \Gamma} \right] \cdot \begin{bmatrix} p_{F1} \\ p_{F2} \end{bmatrix} \quad (22)$$

$$= -\frac{S_B}{1 + S_D} \cdot \frac{1 + \Gamma}{1 - S_D \cdot \Gamma} \cdot S_C \cdot \begin{bmatrix} p_{F1} \\ p_{F2} \end{bmatrix} \quad (23)$$

$$= -\frac{S_B}{1 + S_D} \cdot (p_{F3} + p_{R3}) \quad (24)$$

$$= -\frac{S_B}{1 + S_D} \cdot U_C \quad (25)$$

The value $-S_B/(1 + S_D)$ does not depend on the cavity state nor on any of the observed signals. It is a constant 2 x 1 vector. Therefore the derived signal could be used for estimation of the cavity input voltage changes for all possible klystron settings and cavity states. In order to calculate the amplitude and phase difference, one has to compute the estimated gradient for two measurement points, giving $U_{C.1}$ and $U_{C.2}$. Then the phase shift for the real gradient is equal to:

$$\arg U_{C.2} - \arg U_{C.1} = \arg U_{E.2} - \arg U_{E.1} \quad (26)$$

The relative change of the amplitude is equal to:

$$\frac{|U_{C.2}|}{|U_{C.1}|} = \frac{|U_{E.2}|}{|U_{E.1}|} \quad (27)$$

Basing on the performed measurements it is possible to compute the absolute shift of the cavity field phase and the relative change of the field magnitude.

The simulation

The predicted properties of the RF system were tested in simulation. The model of the system was prepared in the QUCS (Quite Universal Circuit Simulator) environment. The Qucs provides possibility of parameter dependent RF simulations. The circuit modeling the cavity drive system is shown in the *Fig. 9*. The simulation takes two input values: the phase shifter position and the reflection coefficient of the cavity. In the presented simulations the reflection coefficient *G* was modelled using the formula:

$$\Gamma(r, \Phi) = -1 + 0.5 \cdot r + 0.5 \cdot r \cdot \cos \Phi \quad (28)$$

The proposed equation allows to model changes of the G from perfect reflection for $\Phi = 180°$ to perfect match when $\Phi = 0°$ and $r = 1$. The value $r = 0{,}8$ was chosen in order to simulate the non-ideal match of the cavity to the driving waveguide. The *S* parameters of phase shifter are equal to:

$$S_{DH}(\Gamma = -1) = \begin{bmatrix} 0 & \exp(j \cdot \theta) \\ \exp(j \cdot \theta) & 0 \end{bmatrix} \quad (29)$$

The *S* parameters from *T* combiners were extracted from the measurements of the real device. All the other elements were modelled as ideal ones. The results of simulation are found in the *tables 1, 2* and *3*. In the first step, the Black Box matrix is estimated using the algorithm described . For this calculation the power waves, measured for perfect reflection, i.e. for $\Phi = 180°$ are used. The Black Box matrix is equal to:

$$S(\Gamma = -1) = \begin{bmatrix} 0.6576 + 0.57927i & -0.20601 + 0.15829i \\ -0.2061 + 0.15828i & 0.71379 + 0.43806i \end{bmatrix} \quad (30)$$

In the next step the voltage at the cavity input plane is calculated for all data points. The voltage can be directly calculated from the formula:

$$U_C = P_{F3} + P_{R3} \quad (31)$$

The estimated cavity input voltage is calculated from the formula (see formula 21):

$$U_E = S(\Gamma = -1) \cdot \begin{bmatrix} P_{F1} \\ P_{F2} \end{bmatrix} - \begin{bmatrix} P_{R1} \\ P_{R2} \end{bmatrix} \quad (32)$$

In the *Tabl. 4* values of the real and estimated cavity input voltage are presented. The last column contains the ratio U_C/U_E. For all non-zero values this ratio remains constant. Assumption stated was confirmed by the simulation results. It is possible to estimate the non-observable voltage at the cavity input using the forward and reflected waves in both waveguides.

Tabl. 1. The forward and reflected waves in the waveguide I for different shifter positions and cavity reflection coefficients
Tab. 1 Fale - padająca i odbita - w pierwszym falowodzie dla różnych ustawień przesuwnika fazy i współczynnika odbicia wnęki

F[°]	q[°]	Re p_{F1}	Im p_{F1}	Re p_{R1}	Im p_{R1}
0	0	0.0099547	-0.00028651	0.00054663	-0.0028651
0	90	0.010767	-0.00032628	0.0086736	-0.0032628
0	180	0.010807	0.00048642	0.0090713	0.0048642
0	270	0.0099944	0.00052619	0.00094435	0.0052619
90	0	0.010687	8.626e-05	0.0078687	0.0008626
90	90	0.010951	0.00022361	0.010506	0.0022361
90	180	0.010813	0.00048734	0.0091325	0.0048734
90	270	0.01055	0.00034999	0.0064952	0.0034999
180	0	0.010307	0.00080081	0.0040715	0.0080081
180	90	0.010406	0.00039453	0.0050596	0.0039453
180	180	0.010812	0.00049335	0.0091224	0.0049335
180	270	0.010713	0.00089963	0.0081342	0.0089963
270	0	0.0095997	0.00043931	-0.0030029	0.0043931
270	90	0.01023	-0.00013743	0.0032959	-0.0013743
270	180	0.010806	0.00049245	0.0090632	0.0049245
270	270	0.010176	0.0010692	0.0027645	0.010692

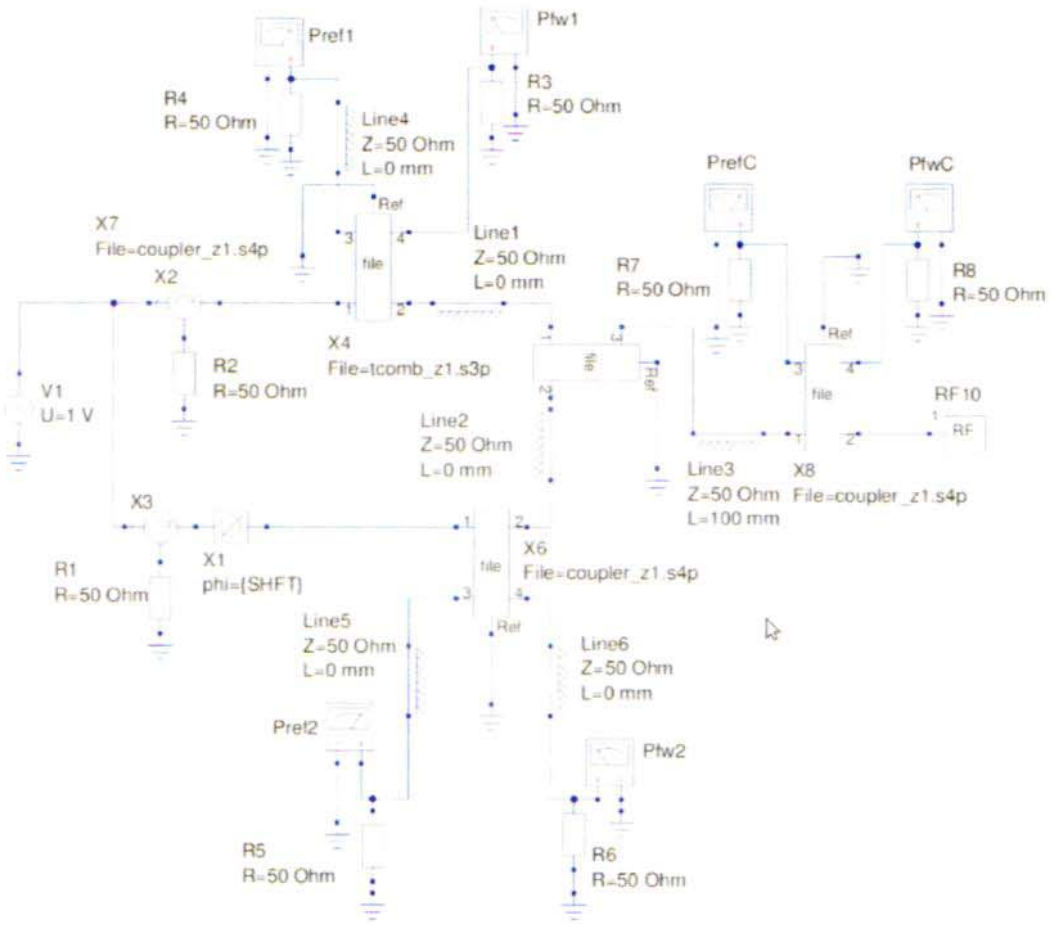

Fig. 9. The QUCS model of the RF-Gun control system.
Rys. 9. Model systemu sterowania działem elektronowym przygotowany przy pomocy programu QUCS

Tabl. 2 The forward and reflected waves in the waveguide II for different shifter positions and cavity reflection coefficients
Tab. 2. Fale - padająca i odbita - w drugim falowodzie dla różnych ustawień przesuwnika fazy i współczynnika odbicia wnęki

F[°]	F[°]	Re p_{F2}	Im p_{F2}	Re p_{R2}	Im p_{R2}
0	0	0.010046	-0.00042552	0.0014585	-0.0042552
0	90	-0.00038715	0.010086	-0.0038715	0.001856
0	180	-0.010898	-0.00034739	-0.0099828	-0.0034739
0	270	-0.00046528	-0.010859	-0.0046528	-0.0095852
90	0	0.010766	-5.4528e-05	0.0086577	-0.00054528
90	90	-0.00020921	0.010629	-0.0020921	0.0072852
0	180	-0.010892	-0.00034646	-0.0099225	-0.0034646
90	270	8.272e-05	-0.01103	0.0008272	-0.011295
180	0	0.010388	0.00064795	0.0048799	0.0064795
180	90	-0.00074688	0.010794	-0.0074688	0.0089434
180	180	-0.010893	-0.00034054	-0.0099328	-0.0034054
180	270	0.0002416	-0.010487	0.002416	-0.0058693
270	0	0.0096924	0.00028818	-0.0020756	0.0028818
270	90	-0.00091815	0.010269	-0.0091815	0.0036914
270	180	-0.010899	-0.00034145	-0.0099911	-0.0034145
270	270	-0.00028851	-0.010322	-0.0028851	-0.0042241

Tabl. 3. The forward and reflected waves at the cavity input plane for different shifter positions and cavity reflection coefficients
Tab. 3. Fale - padająca i odbita - na wejściu wnęki dla różnych ustawień przesuwnika fazy i współczynnika odbicia wnęki

F[°]	F[°]	Re p_{F3}	Im p_{F3}	Re p_{R3}	Im p_{R3}
0	0	-0.0080221	0.011207	-0.0016044	0.0022413
0	90	-0.0095801	0.0016572	-0.001916	0.00033144
0	180	-3.0669e-05	9.9156e-05	-6.1338e-06	1.9831e-05
0	270	0.0015274	0.0096486	0.00030547	0.0019297
90	0	-0.0082238	0.011086	-0.0033662	-0.0093635
90	90	-0.0096218	0.0014968	0.002946	-0.0063711
90	180	-3.2397e-05	9.8776e-05	-4.6322e-05	-5.8901e-05
90	270	0.0013657	0.0096882	-0.0063585	-0.0030513
180	0	-0.0081018	0.01089	0.0080914	-0.010897
180	90	-0.0094632	0.0014585	0.0094618	-0.0014675
180	180	-3.1992e-05	9.7081e-05	3.19e-05	-9.7112e-05
180	270	0.0013294	0.0095283	-0.0013385	-0.009527
270	0	-0.0079069	0.011006	0.0097779	0.00032582
270	90	-0.0094231	0.0016136	0.0047509	0.0050061
270	180	-3.0323e-05	9.7451e-05	7.0643e-05	-2.0927e-05
270	270	0.0014858	0.0094902	0.0050976	-0.0047012

Tabl. 4. The real and estimated voltages at the cavity input plane Tab. 4. Rzeczywiste i estymowane napięcie na wejściu wnęki

F[°]	F[°]	Real voltage U_C	Estimated voltage $U_E(1)$	Voltage Ratio $U_C/U_E(1)$
0	0	-0.009626 + 0.01345i	0.004163 + 0.01012i	0.8018 + 1.281i
0	90	-0.0115 + 0.001989i	-0.002921 + 0.007146i	0.8018 + 1.281i
0	180	-3.68e-05 + 0.000119i	5.382e-05 + 6.242e-05i	0.8018 + 1.281i
0	270	0.001833 + 0.01158i	0.007138 + 0.003037i	0.8018 + 1.281i
90	0	-0.01159 + 0.001723i	-0.0031+ 0.0071i	0.8024 + 1.282i
90	90	-0.006676 - 0.004874i	-0.005074 + 0.002032i	0.8024 + 1.282i
90	180	-7.872e-05 + 3.987e-05i	-5.267e-06 + 5.811e-05i	0.8024 + 1.282i
90	270	-0.004993 + 0.006637i	0.001968 + 0.005127i	0.8024 + 1.282i
180	0	-1.041e-05 - 7.734e-06i	1.105e-14 + 1.13e-14i	-8.106e+08 + 1.288e+08i
180	90	-1.401e-06 - 9.042e-06i	9.54e-15 - 3.316e-15i	1.629e+08 - 8.912e+08i
180	180	-9.279e-08 - 3.05e-08i	-1.56e-15 - 1.728e-14i	2.232e+06 - 5.169e+06i
180	270	-9.104e-06 + 1.278e-06i	-1.903e-14 + 9.296e-15i	4.127e+08 + 1.344e+08i
270	0	0.001871 + 0.01133i	0.007019 + 0.002931i	0.8012 + 1.28i
270	90	-0.004672 + 0.00662i	0.002074 + 0.004949i	0.8012 + 1.28i
270	180	4.032e-05 + 7.652e-05i	5.712e-05 + 4.254e-06i	0.8012 + 1.28i
270	270	0.006583 + 0.004789i	0.005002 - 0.002013i	0.8012 + 1.28i

Summary

In the simulation it was shown that it is possible to compute a parameter which is proportional to the real gradient of the field in the RF-Gun cavity. The presented method may be practically used to estimate the change of this gradient, and to provide useful information for its stabilization. Further research is however required, which should be focussed on applying the presented technique to the control of the RF-Gun via the closed-loop control system. Additionally, a method for eliminating the need for the time-consuming temperature scans has to be developed.

The Authors would like to thank dr Waldemar Koprek and dr Mariusz Grecki from DESY, Hamburg for their support.

References

[1] Photon Injector Test Facility Homepage, http://pitz.desy.de/.
[2] Sekutowicz J.: Multi-cell Superconducting Structures for High Energy e^+ e^- Colliders and Free Electron Laser Linacs. Publishing House of Warsaw University of Technology, Warsaw 2008.
[3] Pozniak K. T.: FPGA technology application in a fast measurement and control system for the TESLA suerconduction cavity of a FLASH free electron laser. Meas. Sci. Technol. 18 (2007) 2336-2347.